Stability of bismuth orthogermanate at high pressure and high temperature

2004 J. Phys.: Condens. Matter 16 8117

(http://iopscience.iop.org/0953-8984/16/46/001)

INSTITUTE OF PHYSICS PUBLISHING JOURNAL OF PHYSICS: CONDENSED MATTER

J. Phys.: Condens. Matter **16** (2004) 8117–8130 PII: S0953-8984(04)85236-6

Stability of bismuth orthogermanate at high pressure and high temperature

Akhilesh K Arora[1,4], **Takehiko Yagi**[2], **Nobuyoshi Miyajima**[2] **and R Gopalakrishnan**[3]

[1] Materials Science Division, Indira Gandhi Centre for Atomic Research, Kalpakkam 603 102, India
[2] Institute for Solid State Physics, Tokyo University, Kashiwanoha, Kashiwa, Chiba 277-8581, Japan
[3] Department of Physics, Anna University, Chennai 600 025, India

E-mail: aka@igcar.ernet.in

Received 20 August 2004, in final form 18 October 2004
Published 5 November 2004
Online at stacks.iop.org/JPhysCM/16/8117
doi:10.1088/0953-8984/16/46/001

Abstract

The stability of cubic bismuth orthogermanate $Bi_4(GeO_4)_3$ is investigated at high pressure (HP) and high temperature (HT) using x-ray diffraction, Raman spectroscopy, and scanning electron microscopy (SEM). At ambient temperature the compound is found to have a bulk modulus of 48 ± 2 GPa and it undergoes amorphization at 12.5 GPa, whereas *in situ* laser heating of amorphous sample in a diamond-anvil cell results in re-crystallization. SEM and Raman spectroscopy of the recovered sample suggest an inhomogeneous sample with regions rich and depleted in Ge, suggesting a decomposition of the parent compound. The decomposition products are identified from the x-ray diffraction. These results show that at HP–HT the compound exhibits complex decomposition paths leading to several mixed oxide phases including α-Bi_2O_3, Bi_2GeO_5, and $Bi_2Ge_3O_9$. The observations of pressure-induced amorphization at ambient temperature in this compound and its decomposition into a mixture of daughter phases at HP–HT are discussed in light of a recent model of pressure-induced amorphization and decomposition.

1. Introduction

Structural phase transition from one crystalline phase to another as a function of thermodynamic parameters such as pressure and temperature arise when the free energy of the new phase becomes lower than that of the original phase. Although the difference in the free energies is the thermodynamic driving force for the transition to take place, often the activation barrier to

[4] Author to whom any correspondence should be addressed.

the transition becomes an important factor in determining the kinetics of the phase transition and leads to hysteresis in the first-order transitions. If the activation barrier is sufficiently high, it can even prevent the phase transition from taking place and the system may finally end up in a disordered/amorphous state. Pressure-induced amorphization (PIA) arising from kinetic hindrance of the equilibrium phase transition [1] was first reported in ice [2] and subsequently in quartz [3] and other systems [4]. Subsequently, other factors such as metastable melting [2], dynamic instability [5], poly-tetrahedral packing [6], and orientational disorder of polyatomic ions [7] have been proposed to be responsible for this. These features are not necessarily all distinct, i.e., more than one may be applicable simultaneously in some cases and hence could be related. It has been recently argued [8] that in many systems, instead of kinetic hindrance of the equilibrium phase transition, 'kinetic hindrance of a decomposition/ disproportionation' of the parent compound into a mixture of dense-packed daughter compounds is the cause of PIA. As the process of nucleation and growth of macroscopic daughter phases is diffusion controlled, pressure-induced solid state decomposition can only occur at elevated temperature. On the other hand, at ambient temperature the system is likely to be trapped in a metastable amorphous (disordered) state while attempting to decompose under the application of pressure [8]. This concept has been applied to several systems [9–13]. In addition, the condition $\Delta V < 0$, where ΔV is the volume change upon decomposition, has been identified as a criterion for PIA at ambient temperature [4, 8]. The reported PIA in zirconium tungstate $Zr(WO_4)_2$ at 2.1 GPa and ambient temperature [14] and pressure-induced decomposition (PID) into mixture of simple oxides ZrO_2 and WO_3 at 0.6 GPa and 1073 K [15] are consistent with this model. On the other hand, in another compound, scandium molybdate, $Sc_2(MoO_4)_3$, with similar network structure, although the predicted amorphization [16] at HP and ambient temperature and decomposition [17] at HP–HT have been confirmed, the decomposition occurred into a mixture of MoO_3 and a more complex mixed oxide $Sc_2Mo_2O_9$ rather than a mixture of simple oxides. In view of this it is of interest to confirm the predictions of the model in other systems with different types of bonding and structure.

Orthogermanates and silicates of bismuth, which crystallize in the eulytite structure, are important scintillation detector materials [18], and when suitably doped with rare earths such as Nd serve as laser materials. These crystals are also photo-refractive and find applications in optical devices [19]. From the photoluminescence and Raman spectroscopic studies bismuth orthogermanate $Bi_4(GeO_4)_3$ has been found to amorphize irreversibly at 12 GPa [20]. However, there is no investigation of its compression behaviour (equation of state) and that of amorphization using x-ray diffraction. In this context it is important to point out that based on Raman spectroscopic studies $Co(OH)_2$ has been found to develop partial or sublattice disorder while it remained overall x-ray crystalline [21, 22]. In view of this one must also ascertain whether $Bi_4(GeO_4)_3$ turns x-ray amorphous or not. Furthermore, quite interestingly $Bi_4(GeO_4)_3$ satisfies the condition of decomposition [11]. Hence it is important to examine whether $Bi_4(GeO_4)_3$ also undergoes PID at HP–HT. In view of the diversity of the decomposition routes in $Zr(WO_4)_2$ and $Sc_2(MoO_4)_3$ it is not straightforward to predict the route a compound may follow during decomposition. It may be pointed out that the Bi_2O_3–GeO_2 binary system, in addition to $Bi_4(GeO_4)_3$, has several mixed oxide phases such as $Bi_{12}GeO_{20}$, Bi_2GeO_5, and $Bi_2Ge_3O_9$ [23], and these have specific volumes of 522.2, 116.3, and 206.6 Å^3 respectively. Hence several decomposition paths may exist in this case. In this paper we report detailed *in situ* high-pressure investigations on $Bi_4(GeO_4)_3$ using x-ray diffraction and Raman spectroscopy in a diamond anvil cell (DAC). The compression behaviour at ambient temperature and the equation of state is obtained. The changes taking place upon laser heating the sample at high-pressure are also examined in the recovered samples using scanning electron microscopy (SEM) in addition to x-ray diffraction and Raman spectroscopy. Characteristic

x-ray emission is used for estimating the composition of phases formed due to HP–HT treatment. The results are discussed in the light of a recent model of amorphization/decomposition [8].

2. Experimental details

Bismuth orthogermanate single crystals were synthesized from high-purity bismuth trioxide and germanium dioxide in 2:3 molar ratio. These were thoroughly mixed in a mortar and pestle, melted in a platinum crucible at 1343 K, and left to homogenize for 12 h, after which the furnace temperature was decreased gradually. Powder x-ray diffraction was used to confirm the purity of the phase. The powdered sample was loaded in a 300 μm hole of preindented stainless steel gasket of the diamond anvil cell. A 4:1 methanol:ethanol mixture was used as the pressure transmitting medium. Ruby fluorescence was used for the estimation of pressure. Raman scattering measurements were carried out using a micro-Raman spectrometer described elsewhere [17]. About 15 mW of power at 514.5 nm wavelength from an argon ion laser was used to excite the sample. X-ray diffraction measurements were made using Mo Kα radiation from a 5.4 kW Rigaku rotating anode generator equipped with a 100 μm collimator. An image plate (IP) was used as the detector. For calibrating the diffraction angle the distance of the IP from the sample (i.e., camera length) was determined by recording the diffraction from silver powder placed on the outer face of the diamond. Average d-spacings were obtained by averaging those from the left and the right patterns. This eliminated the error in d-spacing arising from that in fixing the centre-spot on the image plate.

Double-sided *in situ* laser heating was carried out in the diamond anvil cell using a 100 W CW multimode Nd:YAG laser operating at 1.064 μm. The laser-heating set-up used in the present experiments was very similar to that described elsewhere [24]. The heated area in this system was around 25 μm in diameter. In order to heat the whole area of the sample within the hole of the gasket the DAC was moved in small steps in the x–y plane perpendicular to the direction of the laser beams. On average heating at each point was done for about 30 s and the total heating time was about 30 min. The temperature of the sample during laser heating was estimated by analysing the spectrum of the black-body radiation from the heated spot using a 300 mm focal length monochromator equipped with CCD detector. For laser-heating runs no pressure-transmitting medium was used. Some of the heating runs were also carried out after sandwiching the sample between two sodium fluoride pellets of thickness similar to that of the sample within the hole of the gasket in the DAC. Pressure was also measured after each heating run. Raman and x-ray diffraction measurements were carried out in the DAC as well as on the recovered samples after releasing the pressure. Microscopic observations were made on polished fragments of the recovered samples after embedding them in an epoxy resin using a JSM-5600 scanning electron microscope.

3. Results and discussion

3.1. Compression at ambient temperature

Bismuth orthogermanate crystallizes in the cubic eulytite structure belonging to the space group $I\bar{4}3d$ (220) with four formula units per unit cell [25]. The structure consists of GeO_4 tetrahedra at the S_4 site and bismuth cations on the C_3 axis. Each bismuth ion is coordinated to a distorted octahedron of oxygen atoms of the neighbouring germanate ions [26]. All the diffraction peaks observed in the 0.1 MPa pattern could be indexed to the JCPDS pattern [27] and the cell parameter ($a = 10.528(3)$ Å) thus obtained was found to be in good agreement with

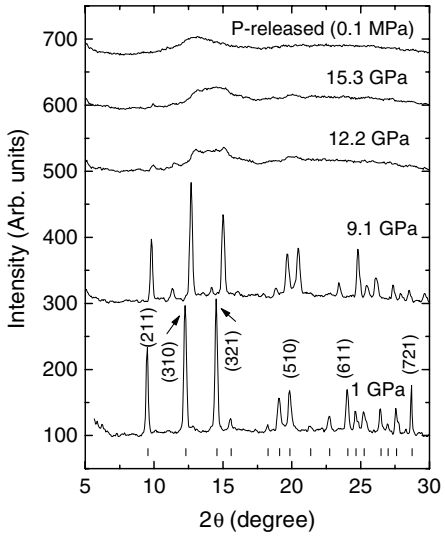

Figure 1. X-ray diffraction pattern of cubic bismuth orthogermanate at different pressures. Indices of some of the prominent peaks are also shown. Vertical bars are the calculated 2θ positions at 1 GPa.

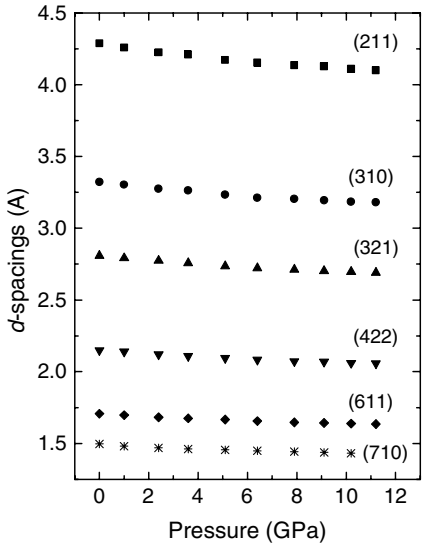

Figure 2. Dependence of selected d-spacings in bismuth orthogermanate on pressure.

the reported data. For the compression run a pressure-transmitting medium of 4:1 methanol–ethanol mixture was used. Figure 1 shows the diffraction patterns at several pressures. At high pressure all the diffraction peaks shifted to higher 2θ. The dependence of the d-spacings on pressure could be followed up to 11 GPa, beyond which diffraction peaks became too weak for unambiguous identification. Figure 2 shows the pressure dependence of selected d-spacings. Note that the decrease of the d-spacings is monotonic and there is no phase transition up to a pressure of 11 GPa. The lattice parameter obtained from the d-spacings also decreases

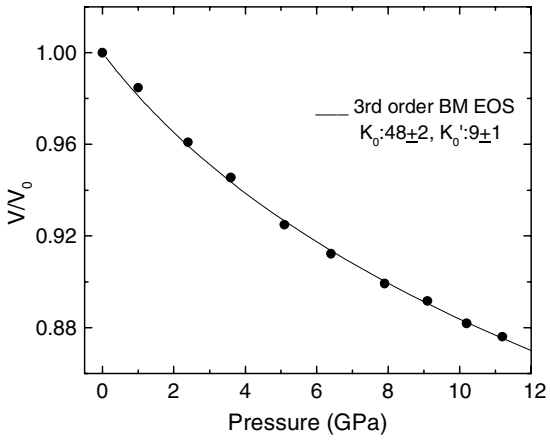

Figure 3. Relative volume as a function of pressure. The solid curve is the fitted third-order Birch–Murghanan equation of state.

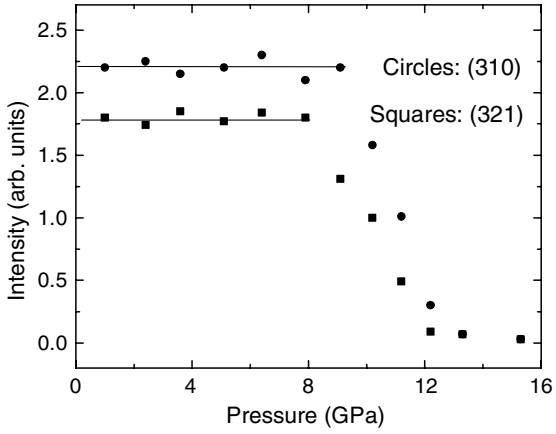

Figure 4. Intensities of the (310) and (321) diffraction peaks as a function of pressure. The intensities are normalized with respect to the background at large 2θ angles.

monotonically to a value of $0.957a_0$ at 11.2 GPa, where a_0 is the lattice parameter in the ambient. The unit cell volume V, normalized to that in the ambient (V_0), is shown in figure 3 as a function of pressure P. The unit cell volume decreased to about 0.876 of the ambient pressure value. The P–V data were fitted to the third-order Birch–Murghanan equation of state [28],

$$P = \tfrac{3}{2}K_0(u^{7/3} - u^{5/3})[1 - \tfrac{3}{4}(4 - K_0')(u^{2/3} - 1)] \quad (1)$$

where $u = V_0/V$. The fit yielded the bulk modulus K_0 as 48 ± 2 GPa and its pressure derivative K_0' to be 9 ± 1. The fitted equation of state is also shown as a continuous curve in figure 3.

Above 10 GPa the intensities of all the diffraction peaks decreased dramatically and the diffraction pattern disappeared completely at 12.5 GPa (figure 1), suggesting amorphization of the sample. When pressure is released to the ambient, the sharp diffraction peaks do not reappear, suggesting that the amorphization is irreversible. The behaviours of the intensities of the prominent difraction peaks (310) and (321) are shown in figure 4. One can see that the

decrease of the intensities is rapid above 9 GPa and the amorphization occurs over a narrow pressure range. This is in contrast to gradual two-stage amorphization found in scandium molybdate [16]. Irreversibility of the amorphization in bismuth orthogermanate was also found in the earlier Raman and photoluminescence study carried out up to 30 GPa using solid argon as the pressure-transmitting medium [20]. In this context it is important to mention that amorphization in isostructural bismuth orthosilicate has been found to be reversible [11]. The irreversibility of amorphization in bismuth orthogermanate under argon pressure-transmitting medium [20] was argued [11] to arise due to the presence of a large non-hydrostatic component of the stress and to the extent of the highest pressure reached (over-driving of amorphization) in the high-pressure run. A need to explore the possibility of reversible amorphization under hydrostatic conditions was also pointed out. In contrast to this speculation the present experiments clearly show irreversibility of the amorphization in bismuth orthogermanate even under near hydrostatic conditions, when pressure is released from 15 GPa. Hence the possible reason for the difference in the behaviour of bismuth orthogermanate and bismuth orthosilicate could be different. The other important difference between these two compounds is the strength of bonding between Ge and O and Si and O. This is also manifest in the phonon frequencies of symmetric stretching (ν_1) and other vibration modes of GeO_4 (818 cm^{-1}) and SiO_4 (991 cm^{-1}) tetrahedra in orthogermanates [29] and orthosilicates [30]. Similarly, the ν_1 mode frequency of GeO_4 tetrahedra in $Bi_{12}GeO_{20}$ (715 cm^{-1}) is found to be significantly lower than that of SiO_4 tetrahedra in $Bi_{12}SiO_{20}$ (785 cm^{-1}) [31]. The fact that the Si–O bond is much harder than the Ge–O bond is also evident from the frequencies of α-quartz being about 1.2 times higher than those of the quartz phase of GeO_2 [32]. Theoretical calculations have shown that the Ge–O force constant is significantly smaller than the Si–O force constant [33]. In addition, it is also comparable to the Bi–O force constant. From these results it emerges that Bi–O and Ge–O bonds in bismuth orthogermanate are of similar strength, while Bi–O and Si–O bonds in bismuth orthosilicate are significantly different. This can bring about a difference in the disordering process/mechanism during amorphization. When a system with widely different bond strengths such as bismuth orthosilicate amorphizes, the Bi–O weaker bond is expected to break while the strongly bound SiO_4 units, though severely distorted, may still remain intact. Thus the disordered state still has some kind of partial memory of local structure/order. Survival of SiO_4 tetrahedral units even in the amorphous state can lead to reordering/recovery to the original structure when pressure is released. On the other hand, if the system consists of bonds with similar strengths such as those in bismuth orthogermanate, then during amorphization both Bi–O and Ge–O bonds can break, leading to completely new local structure in the disordered state with no memory of the original structure. The amorphization in such cases is expected to be irreversible. Thus the reversibility/irreversibility of amorphization can be understood on the basis of the strength of bonding.

The cubic eulytite structure of bismuth orthogermanate is relatively less densely packed as compared with the constituent oxides. This is evident from the specific volumes of $Bi_4(GeO_4)_3$, α-Bi_2O_3 (bismite), and GeO_2 (rutile phase), which are 291.7, 82.63, and 27.67 $Å^3$ respectively. From these data ΔV turns out to be -43.5 $Å^3$, suggesting decomposition to be favourable at high pressure. For high-pressure decomposition, it is reasonable to consider the volume of the rutile phase rather than the quartz phase, because the rutile is the equilibrium high-pressure structure. In addition to decomposition giving rise to a mixture of simple oxides, other decomposition routes leading to a mixture of more complex mixed oxides have also been predicted to be favourable from specific volume considerations [11]. It was pointed out in the recent model of amorphization [8] that a favourable decomposition is also a criterion for predicting PIA. This is because of insufficient kinetics for decomposition at ambient temperature. In view of this, amorphization in this system is understandable.

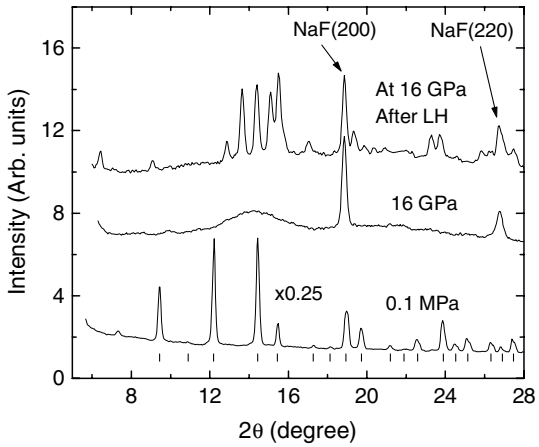

Figure 5. Diffraction pattern of bismuth orthogermanate sample at 16 GPa before and after laser-heating treatment. The cubic pattern of the parent compound at 0.1 MPa is shown for comparison. Vertical bars are the calculated 2θ positions for the cubic phase at the ambient pressure.

3.2. Laser heating of amorphous samples

In order to confirm whether this system indeed undergoes PID at HP–HT, and to identify the actual decomposition products and routes, we carried out high-pressure *in situ* laser heating of the amorphous samples in the diamond-anvil cell at pressures between 15 and 16 GPa. In order to exclude the possibility of reaction of the sample with the pressure-transmitting medium at high temperature, no pressure-transmitting medium was used in the heating runs. Bismuth orthogermanate has a very large mass absorption coefficient ($\sim$92 cm^2 g^{-1}) for Mo Kα radiation and hence the intensities of the diffraction peaks were strongly attenuated when the full thickness ($\sim$75 μm) of the gasket hole was filled with the sample. In order to reduce the attenuation of the x-ray beam, an approximately 25 μm thick pellet of sample was sandwiched between two NaF pellets of similar thickness. This also provided thermal insulation between the sample and the diamond faces. However, some of the laser-heating runs were also done without the NaF sandwich. The diffraction patterns recorded after laser heating the samples with and without the NaF sandwich were found to be identical.

The sample, which was transparent and colourless at 15 GPa to begin with, was found to turn black immediately upon laser heating. After laser heating the sample x-ray diffraction patterns were recorded at high pressure as well as after releasing the pressure. Pressure was also measured after each heating run and was found to be within 0.5 GPa of that before heating. From the spectrum of the incandescent light emitted from the sample, the temperature was estimated to be 1300 ± 100 K for heating with 10 W laser power. No temperature measurement was possible during heating with lower laser powers. Figure 5 shows the diffraction pattern at 16 GPa after heating the sample with a laser power of 10 W. Note that a distinct crystalline pattern different from that of the parent compound emerges as a result of laser heating. When pressure is released, the diffraction pattern does not change. This suggests that either the phase/phases formed as a consequence of laser heating have no structural transition up to 16 GPa or these high-pressure phase/phases can be quenched to the ambient.

Figure 6 shows the Raman spectra of the sample recorded from different regions of the sample recovered after laser heating at 16 GPa, along with those of the parent compound, α-Bi_2O_3, and GeO_2 (quartz type). One can see that the spectra consist of at least two different sets of peaks with different relative intensities. The modes at 449, 562, and 720 cm^{-1} are

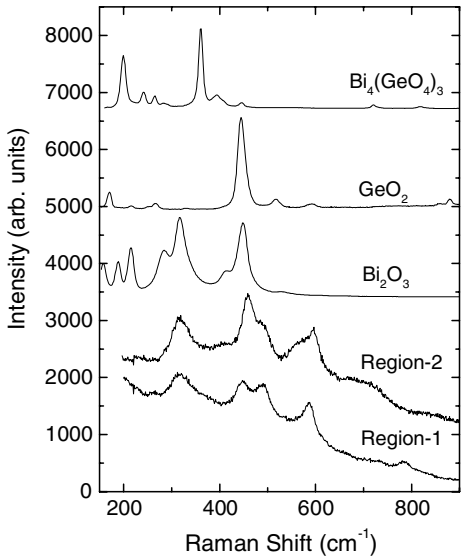

Figure 6. Raman spectra of the sample recovered after laser heating at 16 GPa in two different regions of the sample. Spectra of Bi_2O_3, GeO_2 and the parent compound are also shown for comparison.

Table 1. Frequencies of the Raman peaks (in cm^{-1}) observed in the samples recovered after laser heating the bismuth germanate in a DAC. Characteristic frequencies of Bi_2O_3 and GeO_2 are also given for comparison. The frequencies in bold are the strong peaks.

Recovered sample	Bi_2O_3	GeO_2
	158	170
	189	216
	215	226
	284	
317	**317**	
	414	
449	**448**	**445**
459		
490	528	517
562		
590		592
720		
784		

strong in one spectrum while those at 490, 590, and 784 cm^{-1} are prominent in the other. This suggests that the sample has turned inhomogeneous after laser heating. Furthermore, the Raman peaks of the recovered sample do not correspond to the parent compound. Table 1 compares the positions of the Raman peaks found in the recovered sample with those of Bi_2O_3 and GeO_2. Note that the most prominent peaks of Bi_2O_3 (317 and 448 cm^{-1}) [34] are present in the spectra of the recovered sample, indicating that the parent compound could have undergone a pressure-induced decomposition into a mixture of Bi_2O_3 and other compounds. In analogy with the examples of $Zr(WO_4)_2$ and $Sc_2(MoO_4)_3$ [15, 17], the other decomposition product/products could be GeO_2 or other mixed oxides of Bi and Ge. As mentioned earlier,

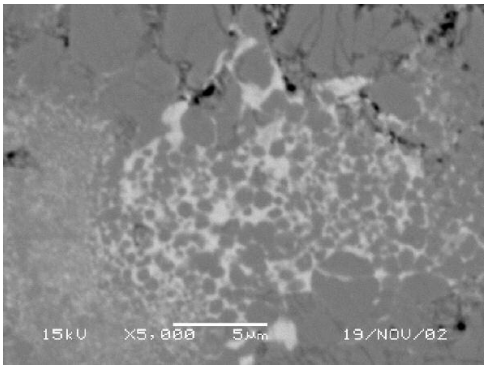

Figure 7. Scanning electron micrograph (back-scattered electron image) of the recovered sample after laser heating bismuth orthogermanate at 16 GPa. Bright regions are rich in bismuth, while the dark regions have more germanium.

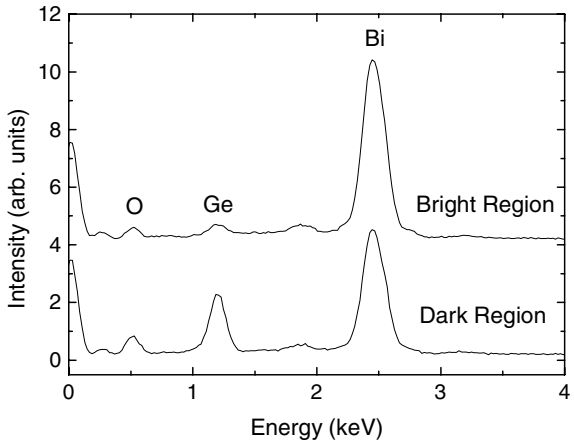

Figure 8. Energy dispersive x-ray emission spectra from bright and dark regions of the sample recovered after laser heating. Peaks labelled Bi, Ge, and O correspond to Bi-M, Ge-L, and O-K x-ray emission lines from the respective atoms.

other mixed oxides are $Bi_{12}GeO_{20}$, Bi_2GeO_5, and $Bi_2Ge_3O_9$. Raman spectra of Bi_2GeO_5 and $Bi_2Ge_3O_9$ are not known. One can also see from table 1 that the only prominent Raman peak of GeO_2 at 445 cm^{-1} is close to that found in the recovered sample. Thus the presence or absence of GeO_2 as one of the decomposition products cannot be concluded from the Raman data alone. It may also be pointed out that the observed Raman peaks also do not correspond to those of the rutile phase of GeO_2 (680, 702, and 870 cm^{-1}) [32] and cubic $Bi_{12}GeO_{20}$ (273, 338, and 542 cm^{-1}) [31].

In order to confirm whether the sample had really turned inhomogeneous as a result of laser heating, we examined the fragments of the recovered sample in a scanning electron microscope. Figure 7 shows the back-scattered electron image. The bright regions are a micrometre or less in size. From the elemental image, obtained from the characteristic x-ray emission, the bright regions were found to be rich in Bi while the dark regions were rich in Ge, confirming that the sample had indeed undergone decomposition into compounds that are rich in Bi and Ge. Figure 8 shows the energy dispersive x-ray emission spectra from regions/phases with different

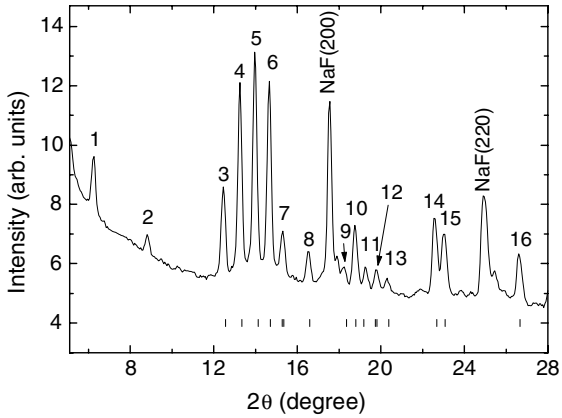

Figure 9. X-ray diffraction pattern of the sample recovered after laser heating at 16 GPa. Peaks numbered 1–16 are indexed in table 2. The calculated 2θ positions are shown as vertical bars.

contrasts. Note that the bright regions are nearly free from Ge, suggesting that this could be predominantly Bi_2O_3 phase. On the other hand, the dark region, which is rich in Ge, still has a significant amount of Bi present in it. This implies that the phase/phases present in this region are the mixed oxides of Bi and Ge, with bismuth stoichiometry different from that of the parent compound.

In order to identify the compounds/phases present in the laser-heated sample we analysed the diffraction patterns of the recovered samples. The possible decomposition products are Bi_2O_3, $Bi_{12}GeO_{20}$ (cubic, space group $I23(197)$), Bi_2GeO_5 (orthorhombic, space group $Cmc2_1(36)$), $Bi_2Ge_3O_9$ (hexagonal, space group $P6_3/m(176)$), and GeO_2. Figure 9 shows the diffraction pattern of the recovered sample. None of the diffraction peaks corresponded to the parent phase, suggesting that the transformation is complete. Several peaks of the recorded pattern were found to correspond to the monoclinic (α) phase, space group $P21/c$ (14), of Bi_2O_3. This phase is most dense among all the known phases of Bi_2O_3. Germanium dioxide has α-quartz type structure in the ambient [35] and has several high-pressure polymorphs such as rutile type [36], orthorhombic [37], and monoclinic [38]. The remaining diffraction peaks of the recovered sample correspond neither to any of the known phases of GeO_2 nor to $Bi_{12}GeO_{20}$ [39]. However, peaks corresponding to both Bi_2GeO_5 and $Bi_2Ge_3O_9$ phases were present. The observed d-spacings were used for obtaining the cell parameters of these phases and the calculated d-spacings are given in table 2 along with their indices. The presence of unindexed lines suggests that there could be another mixed oxide phase. As the x-ray diffraction pattern corresponds to a multi-phase system, a more detailed analysis of the phases in terms of profile fitting is difficult. Thus the x-ray diffraction measurements suggest that Bi_2O_3, Bi_2GeO_5 and $Bi_2Ge_3O_9$ and an unidentified phase are the decomposition products. The calculated cell parameters are compared with those reported in the JCPDS data in table 3. The small number of diffraction peaks used for obtaining the cell parameters of each of the phases resulted in rather large standard error in the calculated cell parameters. The disagreement between the fitted and reported cell parameters may be due to a slight departure of the stoichiometry of the daughter phases from their ideal value arising from factors such as dissolution of Ge in Bi_2O_3 etc. This may also be the reason for marginal disagreement between the observed and the calculated d-spacings. Availability of synchrotron radiation, with better angular resolution in the x-ray diffraction patterns, would be useful in discriminating among resulting daughter compounds.

Table 2. Observed and calculated d-spacings in the sample recovered after laser heating bismuth orthogermanate in a DAC. Different phases are labelled as B3, α-Bi_2O_3; B5, Bi_2GeO_5; and B9, $Bi_2Ge_3O_9$.

	Observed d-spacings	Calculated d-spacings	Index
1	6.461	?	—
2	4.590	?	—
3	3.258	3.240	B3 (120)
4	3.063	3.055	B5 (311)
5	2.909	2.887	B9 (201)
6	2.772	2.770	B5 (020)
7	2.656	2.668	B3 (200)
		2.657	B5 (002)
8	2.462	2.259	B9 (004)
9	2.232	2.224	B9 (211)
10	2.171	2.171	B3 (131)
11	2.114	2.129	B3 (122)
12	2.060	2.071	B9 (212)
		2.061	B5 (421)
13	2.008	2.005	B3 (023)
14	1.809	1.804	B3 (202)
15	1.775	1.774	B3 (−142)
16	1.538	1.538	B3 (−134)

Table 3. Cell parameters obtained from the observed d-spacings for different phases in the recovered sample. α-Bi_2O_3, monoclinic; Bi_2GeO_5, orthorhombic; $Bi_2Ge_3O_9$, hexagonal.

Phase	Fitted cell parameters	JCPDS data
	α-Bi_2O_3	
a	5.77(5)	5.85
b	8.16(3)	8.17
c	7.48(4)	7.512
β	112.5(5)	112.99
V_0	325(3)	330.5
	Bi_2GeO_5	
a	15.16(9)	15.698
b	5.54(1)	5.500
c	5.31(1)	5.387
V_0	446(3)	465.1
	$Bi_2Ge_3O_9$	
a	6.98(3)	7.00
c	9.84(7)	9.783
V_0	414(4)	415.1

From the structural information about different mixed oxide phases, we now attempt to identify the decomposition reaction applicable in the present case. In addition to the decomposition of bismuth orthogermanate into a mixture of simple oxides according to the reaction

$$\text{A:} \qquad Bi_4(GeO_4)_3 \rightarrow 2Bi_2O_3 + 3GeO_2, \tag{2}$$

Table 4. Bismuth to germanium atom ratio obtained from energy dispersive x-ray analysis of different laser-heated samples. This ratio is given for pure phases for comparison. The calculated fraction of $Bi_2Ge_3O_9$ in the dark region ($Bi_2GeO_5 + Bi_2Ge_3O_9$) is also given.

Compounds/products	Bi/Ge ratio	Fraction of $Bi_2Ge_3O_9$
Laser-heated samples		
Sample I		
Bright region	9.33	—
Dark region	1.26	0.3
Sample II		
Bright region	5.47	—
Dark region	0.98	0.5
Sample III		
Bright region	9.1	—
Dark region	1.43	0.2
Pure phases		
Bi_2O_3	∞	
$Bi_{12}GeO_{20}$	12	
Bi_2GeO_5	2	
$Bi_4(GeO_4)_3$	1.33	0.25
$Bi_2Ge_3O_9$	0.67	1
GeO_2	0	

four more decomposition reactions are possible. These are

$$\text{B:} \quad 3Bi_4(GeO_4)_3 \rightarrow Bi_{12}GeO_{20} + 8GeO_2, \tag{3}$$

$$\text{C:} \quad Bi_4(GeO_4)_3 \rightarrow 2Bi_2GeO_5 + GeO_2, \tag{4}$$

$$\text{D:} \quad 2Bi_4(GeO_4)_3 \rightarrow 3Bi_2GeO_5 + Bi_2Ge_3O_9, \tag{5}$$

and

$$\text{E:} \quad Bi_4(GeO_4)_3 \rightarrow Bi_2O_3 + Bi_2Ge_3O_9. \tag{6}$$

From the specific volumes of various mixed oxide phases of Bi and Ge, the volume changes upon decomposition for these five reactions A, B, C, D, and E turn out to be -14.7%, -14.8%, -11.6%, -4.9%, and -0.3% respectively. As compelling evidence for the formation of GeO_2 is not found, reactions A, B, and C may not be applicable. However, incorporation of some amount of GeO_2 in Bi_2O_3 cannot be ruled out. One can see from equations (2) to (6) that the products Bi_2O_3, Bi_2GeO_5, and $Bi_2Ge_3O_9$ can emerge if reactions D and E proceed simultaneously. These reactions can give rise to the presence of Bi_2O_3, Bi_2GeO_5 and $Bi_2Ge_3O_9$ in different proportions. The Ge-rich dark region, which also has a significant amount of Bi in it, could hence be a mixture of Bi_2GeO_5 and $Bi_2Ge_3O_9$.

In order to obtain the stoichiometry of these phases the characteristic x-ray emission spectra from bright and dark regions were analysed semi-quantitatively. The bismuth to germanium atom ratio was obtained by assuming its value to be 1.33 in the parent compound, which was also measured using energy dispersive x-ray analysis. Table 4 gives the Bi/Ge atom ratio obtained from the dark and bright regions of recovered samples from different heating runs. Note that the Bi/Ge ratios for the bright and the dark regions are widely different. The large Bi/Ge ratio found in the bright region suggests that Bi_2O_3 coexists with another Bi-rich mixed oxide phase containing a small amount of GeO_2 similar to $Bi_{12}GeO_{20}$. On the other hand, the Bi/Ge ratio in the dark region ranges between 0.98 and 1.43 in different samples. Assuming

that the dark region consists of a mixture of Bi_2GeO_5 and $Bi_2Ge_3O_9$ phases, the estimated fraction of the $Bi_2Ge_3O_9$ phase in the dark region is also given in table 4 for different samples. More detailed quantitative analyses of the individual phases within the dark and the bright regions were not possible as these regions were too small. Thus the results suggest that the dark regions could be composed of a mixture of Bi_2GeO_5 and $Bi_2Ge_3O_9$, while the bright regions contain Bi_2O_3 and another unidentified mixed oxide phase that is Bi rich and contains some amount of Ge in it.

In view of the present results a discussion on the issue 'why a given system follows a specific decomposition route of decomposition' is in order. In the present compound bismuth orthogermanate, although decomposition route 'A' corresponds to the maximum change in volume, it is not preferred under the present pressure and temperature conditions. On the other hand, decomposition paths 'D' and 'E' leading to incomplete/partial decomposition seem to be more favourable. Similar incomplete decompositions have also been found to occur in other systems [17, 40, 41]. In this context it is important to point out that the difference in the free energy ΔG between the parent compound and the decomposition products is the thermodynamic driving force that drives the system towards the equilibrium phase(s). On the other hand, the activation barrier Δg decides whether a specific decomposition reaction is able to proceed at a given temperature. From these considerations one can say that the activation barrier for path 'A' is probably higher than those of reactions 'D' and 'E' and a complete decomposition of the parent compound into mixture of simple oxides could possibly occur at still higher temperatures. In addition to these considerations the extent of non-hydrostatic pressure conditions during laser heating, arising from experimental constraints, could also be a factor that could force one specific decomposition path instead of another. Calculations of free energies of different daughter compounds and those of activation barriers for different paths are expected to provide further insight into the phenomenon of pressure-induced decomposition.

4. Summary and conclusions

In situ x-ray diffraction and Raman spectroscopic studies are carried out on the nonlinear optical material cubic bismuth orthogermanate at high pressure and high temperature in a YAG laser-heated diamond anvil cell. The analysis of the P–V data at ambient temperature yielded a bulk modulus of 48 ± 2 GPa. As predicted by a recent model of amorphization/decomposition, this compound exhibits an irreversible amorphization at 12.5 GPa. On the other hand, at 16 GPa and 1300 K it follows complex decomposition paths to yield several decomposition products. Some of the daughter phases are identified as Bi_2O_3, Bi_2GeO_5, and $Bi_2Ge_3O_9$.

Acknowledgments

It is a pleasure to thank Mr V S Sastry and Dr P C Sahu for fruitful discussions and Ms F Sakai for help in SEM that was carried out using facilities of the Materials Design and Characterization Laboratory, ISSP, University of Tokyo. AKA acknowledges JSPS for travel support and local hospitality at ISSP. AKA thanks Dr B Viswanathan for interest in the work, Dr S L Mannan for support and Dr Baldev Raj for encouragement.

References

[1] Mishima O, Calvert L D and Whalley E 1985 *Nature* **314** 76
[2] Mishima O, Calvert L D and Whalley E 1984 *Nature* **310** 393
[3] Hazen R M, Finger L W, Hemley R J and Mao H K 1989 *Solid State Commun.* **72** 507

[4] Arora A K 2002 *High Pressure Phenomena* (*International School of Physics 'Enrico Fermi'* vol 147) ed R J Hemley, G L Chiarotti, M Bernasconi and L Ulivi (Amsterdam: IOS Press) p 545 and references therein
[5] Tse J S and Klug D D 1991 *Phys. Rev. Lett.* **67** 3559
[6] Winters R R, Serghiou G C and Hammack W S 1992 *Phys. Rev.* B **46** 2792
[7] Sakuntala T, Arora A K, Shekar N V C and Sahu P C 1998 *Europhys. Lett.* **44** 728
[8] Arora A K 2000 *Solid State Commun.* **115** 665
[9] Ravindran T R, Arora A K and Mary T A 2001 *J. Phys.: Condens. Matter* **13** 11573
[10] Grzechnik A, Crichton W A, Syassen K, Adler P and Mezouar M 2001 *Chem. Mater.* **13** 4255
[11] Ravindran T R, Arora A K and Gopalakrishnan R 2002 *J. Phys.: Condens. Matter* **14** 6579
[12] Pereira A S, Perottoni C A and da Jornada J H A 2003 *J. Raman Spectrosc.* **34** 578
[13] Dimitriev V, Sinitsyn V, Dilanian R, Machon D, Kuznetsov A, Ponyatovsky E, Lucazeau G and Weber H P 2003 *J. Phys. Chem. Solids* **64** 307
[14] Ravindran T R, Arora A K and Mary T A 2000 *Phys. Rev. Lett.* **84** 3879
[15] Amores J M G, Amador U, Moran E and Franco M A A 2000 *Int. J. Inorg. Mater.* **2** 123
[16] Arora A K, Nithya R, Yagi T, Miyajima N and Mary T A 2004 *Solid State Commun.* **129** 9
[17] Arora A K, Yagi T, Miyajima N and Mary T A 2004 *J. Appl. Phys.* at press
[18] Weber M J and Monochamp R R 1973 *J. Appl. Phys.* **44** 5495
[19] Hall D, Newhause N, Borelli N, Dumbaugh W and Weidman D 1989 *Appl. Phys. Lett.* **54** 1293
[20] Zou G, Liu Z, Wang L, Zhao Y, Cui Q and Li D 1991 *Phys. Lett.* A **156** 450
[21] Nguyen J H, Kruger M B and Jeanloz R 1997 *Phys. Rev. Lett.* **78** 1936
[22] Shieh S R and Duffy T S 2002 *Phys. Rev.* B **66** 134301
[23] Corsmit G, van Driel M A, Elsenaar R J, van de Guchte W, Hoogenboom A M and Sens J C 1986 *J. Cryst. Growth* **75** 551
[24] Yagi T, Kondo T, Watanuki T, Shimomura O and Kikegawa T 2001 *Rev. Sci. Instrum.* **72** 1293
[25] Fisher P and Waldner F 1982 *Solid State Commun.* **44** 657
[26] Segal D J, Santoro R P and Newnham R E 1966 *Z. Kristallogr.* **123** 73
[27] Powder Diffraction File (JCPDS Int. Center Diff. Data, Swarthmore, 1982) Card# 34-0416
[28] Li J, Mao H K, Fei Y, Gregoryanz E, Eremets M and Zha C S 2002 *Phys. Chem. Minerals* **29** 166
[29] Beneventi P, Bersani D, Lottici P P and Kovacs L 1995 *Solid State Commun.* **93** 143
[30] Couzi M, Vignalou J R and Boulon G 1976 *Solid State Commun.* **20** 461
[31] Venugopalan S and Ramdas A K 1972 *Phys. Rev.* B **5** 4065
[32] Scott J F 1970 *Phys. Rev.* B **1** 3488
[33] Wojdowski W 1985 *Phys. Status Solidi* b **130** 121
[34] Narang S N, Patel N D and Kartha V B 1994 *J. Mol. Struct.* **327** 221
[35] Jorgensen J D 1978 *J. Appl. Phys.* **49** 5473
[36] Hazen R M and Finger L W 1981 *J. Phys. Chem. Solids* **42** 143
[37] Powder Diffraction File (JCPDS Int. Center Diff. Data, Swarthmore, 1982) Card#35-1370
[38] Haines J, Leger J M and Chateau C 2000 *Phys. Rev.* B. **61** 8701
[39] Powder Diffraction File (JCPDS Int. Center Diff. Data, Swarthmore, 1982) Card#34-0096
[40] Arora A K and Sakuntala T 2000 *High Pressure Res.* **17** 1
[41] Hegenbart W, Rau F and Range K J 1981 *Mater. Res. Bull.* **16** 413